Experimental Investigation on Spray Characteristics of Pressure-Swirl Atomizers for a Small-Sized Jet Engine

L. Durdina*, J. Jedelsky and M. Jicha
Faculty of Mechanical Engineering, Brno University of Technology, Czech Republic
y107165@stud.fme.vutbr.cz, jedelsky@fme.vutbr.cz and jicha@fme.vutbr.cz

Abstract

This study investigated characteristics of sprays generated with two geometrically different pressure-swirl atomizers for a small-sized aviation turbine engine using Particle Image Velocimetry (PIV) and Phase-Doppler Anemometry (PDA). The former nozzle is a spill-return type; the latter one is the intended upgrade without the spill return. Single-camera and stereoscopic PIV measurements yield distribution of mean velocity measured in an axial cross section of the spray cone. PDA measurements yield drop-size distribution and axial velocity data. Performed measurements revealed significant differences in spray characteristics of the measured nozzles investigated in the same operating regimes on a cold test bench. These differences are discussed in detail. Analysis of differences between the two nozzles elucidates the possible impact of the nozzle replacement on the combustion process. This study provides an extensive database for validation of numerical models of the tested nozzles.

Introduction

Research and development of aerospace propulsion systems has been recently strongly motivated by the ACARE goals of environmental capability. European aviation has pledged to reduce NO_x emissions by 80% by 2020 via improvements of the combustor technology [1]. Characteristics of fuel nozzles, such as the spray dispersion angle, drop-size and velocity distribution and evaporation have a significant influence on the combustor performance. Spray quality affects stability limits, combustion efficiency and pollutant emission levels. Good atomization quality promotes the fuel evaporation and decreases the demand of ignition energy [2].

Pressure-swirl atomizers (simplex atomizers) are widely used in industrial and domestic burners, rocket engines, gas turbine combustors and many other engineering areas thanks to their simple design, low power demands and good atomization characteristics.

The operating principle of pressure-swirl atomizers relies on the conversion of liquid pressure into kinetic energy to achieve high relative velocity between the liquid emerging from a nozzle with respect to the surrounding gas. Inside the nozzle, liquid is fed through tangential ports into a swirl chamber mounted upstream the discharge orifice. The swirling liquid flow under the action of the centrifugal force creates and air-cored vortex in the swirl chamber. The liquid flows through the discharge orifice and spreads in the form of a conical liquid film. This thin layer of liquid is prone to propagation of instabilities within the liquid as well as on the liquid surface, which are caused by the high slip velocity between the liquid sheet and the ambient gas. The instabilities cause the breakup of the liquid sheet into ligaments and then into drops in the form of a hollow cone spray. Further disintegration of drops into smaller droplets occurs further downstream from the nozzle orifice and is driven by the collision between droplets and the action of aerodynamic forces [3].

A drawback of the simplex nozzles is the poor atomization quality for low inlet pressures. This disadvantage has been overcome by the spill-return nozzles, which basically are simplex nozzles with a passage in the rear wall of the swirl chamber (Fig. 2). This passage is connected via a spill line with the fuel tank. When the spill is closed, the atomizer operates as a standard simplex nozzle. Usually a high liquid flow rate is maintained in the feed line; the amount of the discharged liquid is controlled by a valve located in the spill line. Studies have shown that the liquid sheet thickness and the size of droplets that emerge after its breakup decrease with increasing inlet flow rate and do not depend on the flow rate of the discharged liquid. Spill-return atomizers have better atomization quality than simplex nozzles for low discharge flow rates, when the major fraction of the inlet flow rate is diverted to the spill return. However, the spray cone angle varies with the changes in spill-return flow rate which has a negative influence on combustion efficiency. Another drawback is the complicated metering of the flow rate. For these reasons, interest in this atomizer type for aircraft engine combustors has declined [2].

The investigation of spray characteristics and performance of simplex nozzles has been the objective of a number of studies over the last decades. Pioneering studies of the liquid film instabilities and breakup of liquid sheets generated by swirl atomizers were performed by Taylor [4] and Squire [5]. Rizk and Lefebvre [6, 7] stud-

* Corresponding author: y107165@stud.fme.vutbr.cz

ied internal flow and spray characteristics of pressure-swirl atomizers. Wang and Lefebvre [8, 9] further studied mean drop sizes and influence of ambient air pressure on pressure-swirl atomization. More recent experimental studies have focused on the improvement of spray characteristics using advanced laser diagnostic techniques, such as Phase-Doppler Anemometry (PDA) [10-12] and Laser Induced Fluorescence (LIF) [13, 14], and high-speed camera measurements [15].

Spill-return nozzles have been investigated in a smaller scale than simplex nozzles. An early implementation of a fuel system for a jet engine with spill control was described by Carey [16]. Rizk and Lefebvre [17, 18] investigated spray characteristics and drop-size distribution of spill-return nozzles with kerosene as the test liquid. Most recently, Nasr et al. [19] has developed a new spill-return atomizer which can produce a fine spray for very low flow rates.

The present study is completely experimental. Measurements of droplet size and velocity distribution were carried out by means of laser diagnostic techniques – Particle Image Velocimetry (PIV) and PDA. The objective was to investigate the spray characteristics of two miniature pressure-swirl atomizers for a small-sized jet engine designed for experimental aircraft and gliders. The former nozzle (Nozzle 1) is a spill-return type which had been used for several decades. The latter one is the intended upgrade in the form of a newly developed simplex nozzle without spill return (Nozzle 2). Analysis of the differences between these two nozzles elucidates the possible impact of the nozzle replacement on the combustion process. This study provides an extensive database for validation of numerical models of the tested nozzles.

Experimental Methods

The apparatus for investigation of spray characteristics is shown schematically in Figure 1. Aviation kerosene Jet A-1 was pumped from a tank through the mass flow meter Siemens Mass 2100 and was injected vertically into the ambient air at room temperature and atmospheric pressure. The nozzle was mounted in a holder above a cylindrical collecting vessel with mist extraction. The nozzle holder was equipped with a shut-off valve for the spill line. Flow rate and gauge pressure in the spill line were controlled with a rotameter equipped with

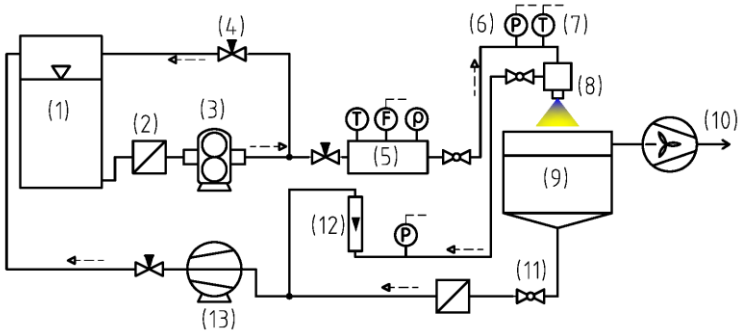

Figure 1 Test rig: (1) fuel tank, (2) filter, (3) gear pump, (4) needle valve, (5) mass flow meter, (6) pressure sensor, (7) temperature sensor, (8) atomizer in a holder, (9) collecting vessel, (10) axial fan and mist extraction, (11) ball valve, (12) rotameter, (13) fuel pump.

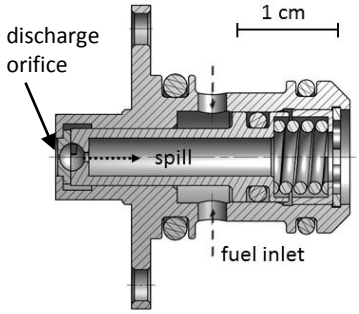

Figure 2 Section view of the spill-return nozzle (Nozzle 1).

a fine metering valve. Collected fuel was pumped by a solid state pump back into the tank. Dashed lines leading from the instruments represent signal outputs for the remote data display. The nozzles were tested at several inlet- and spill line pressure settings. These pressure values are in accordance with the real operating conditions in the engine combustor from idle to maximum power setting (Tab. 1).

Table 1 Operating regimes of the tested nozzles.

Regime	*Nozzle 1*		*Nozzle 2*
no.	Inlet pressure [kPa]	Spill line pressure [kPa]	Inlet pressure [kPa]
1	200	50	200
2	340	0	340
3	690	0	690
4	1000	0	1000
5	1000	400	-

Drop size and velocity were measured using a 1D Dantec PDA system. This 1D system is equipped with the Ion Laser Technology 5500A-00 Ar-Ion$^+$ laser (max. power output 300 mW). The spectral line 514.5 nm of the CW-laser beam with power up to 40 mW and horizontal polarization is split, using the 58N10 transmitting optics, into 2 parallel beams 60 mm distant. The focal length of the transmitting lens is 500 mm, which results in a

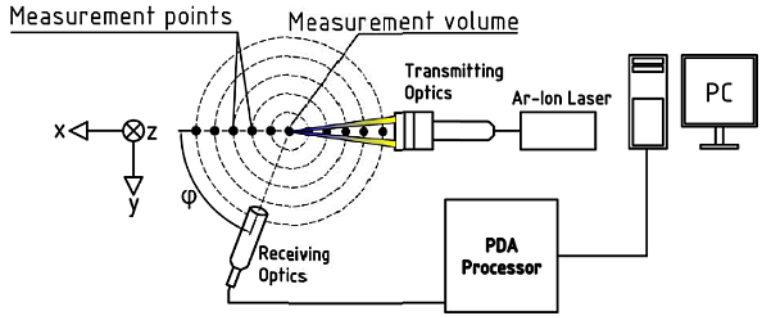

Figure 1 Experimental setup for the PDA measurements.

half-intersection angle between the beams of 3.43°. The frequency of one of the beams is shifted by 40 MHz. This configuration leads to a fringe separation of 4.3 μm. First-order refracted light is collected using Dantec 57X10 receiving optics equipped with three photo-detectors. The focal length of the receiving lens is 500 mm and the scattering angle φ was set to 69°. The setup enables us to measure the drop size up to 220 μm. A Dantec 58N50 signal processor was set to measure velocity within the range of -26 to 26 m/s at 12 MHz bandwidth. The obtained data were evaluated using BSA Flow Software v2.1. Experimental setup for PDA measurements is shown in Fig. 3. Radial scans of the spray profiles were carried out in two planes – 25 and 50 mm downstream of the discharge orifice with 10 mm distance between the measurement points.

Planar single-camera and stereoscopic PIV systems from TSI (Fig. 4) were used for measurements of the velocity distribution and evaluation of the statistical properties of the flow field. A vertical laser light sheet of approximately 1 mm thickness is produced by a double-pulse Nd:YAG laser (NewWave Research Gemini, 50 mJ per pulse, max. repetition rate 15 Hz) conditioned through a cylindrical lens. The light sheet illuminated an axial cross section of the spray. In case of the single-camera system, a CCD camera is oriented perpendicular to the

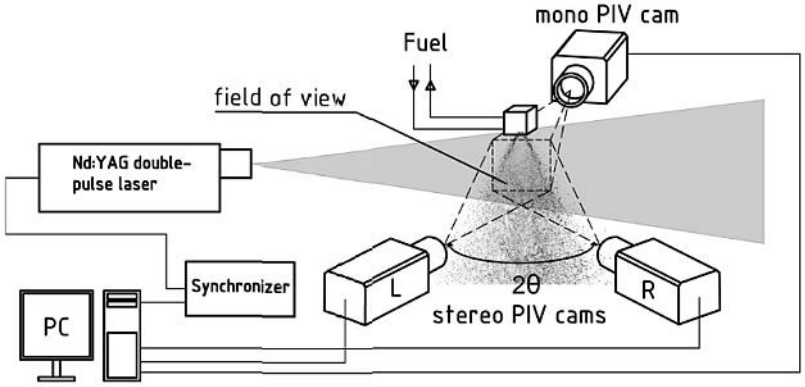

Figure 4 Experimental setup for the PIV measurements.

light sheet and the processed data yields 2-component velocity field. In the stereoscopic configuration, cameras were placed on the same side of the light sheet (back- and forward light scatter) with the full stereoscopic viewing angle 2θ = 80°. This angle provides sufficient accuracy for the estimation of the out-of-plane velocity component [20]. Data processing of the stereoscopic measurements yields 3-component velocity vector field. Timing of the PIV system is controlled by a TSI LaserPulse synchronizer in concert with an acquisition computer. The PIV images were acquired and processed by TSI Insight 3G 10.0 software package. For each experimental run, 1000 paired images were captured and subsequently interrogated using a recursive cross-correlation algorithm. The first pass and second pass spot sizes were 64 x 64 px and 32 x 32 px respectively. Each of the experimental runs, differing in the inlet pressure, required different time delay between laser pulses (from 20 to 50 μs) in order

to minimize the out-of-plane motion of particle images between the paired captures, as well as the in-plane loss of correlation due to large particle displacement at higher velocities.

Results and Discussion

Figure 5 shows axial sections of the sprays generated by both nozzles for each operating regime; these photographs were obtained from the single-camera PIV measurements. Figures 5a to 5e concern Nozzle 1, whereby figures 5a and 5e show the regimes with the spill return valve open. Figures 5f to 5i concern Nozzle 2.

It can be observed that Nozzle 1 generates a noticeable fraction of large drops dispersed in the whole spray cone at lower inlet pressures (Fig. 5a to 5c). Figure 5a shows the conical liquid sheet emerging from the nozzle orifice. This tulip shape terminates in a ragged edge where the fuel disintegrates into ligaments and droplets. With increasing pressure differentials, spray core is formed by smaller droplets due to the drag force caused by gas entrainment towards the spray core and larger droplets can be observed at the spray periphery (Fig. 5c, 5d). Comparing figures 5d and 5e, we can see that the increase in spill flow decreases the droplet size in the spray core. This is due to the decreasing thickness of the liquid sheet. Flow rate regulation via the spill return valve also causes changes in spray cone angle. Cone angles described here were measured as the maximum cone angle 2θ, defined as the angle between the slopes of the liquid sheet close to the discharge orifice [3]. Cone angles were estimated from averaged PIV captures shown in Figure 6 and are summarized in Table 2. Increase in spray cone angle is noticeable at both tested regimes with spill flow regulation compared to the regimes with closed spill return (Fig 5a, 5e). Nozzle 1 exhibits a slight increase in spray cone angle with increasing gauge pressure until the inlet pressure reaches approx. 600 kPa. Higher increase in pressure does not cause further increase in cone angle; thus the cone angle is defined by the internal geometry of the nozzle.

Nozzle 2 exhibits a strong dependence of spray characteristics on the pressure differential. At the lowest tested gauge pressure (Fig. 5f), liquid sheet is contracted by the surface tension force and forms an onion-shaped bubble which collapses close to the spray axis. Therefore, drops are concentrated around the spray axis, creating a full cone spray. With increasing kinetic energy and pressure differential liquid sheet straightens and diminishes

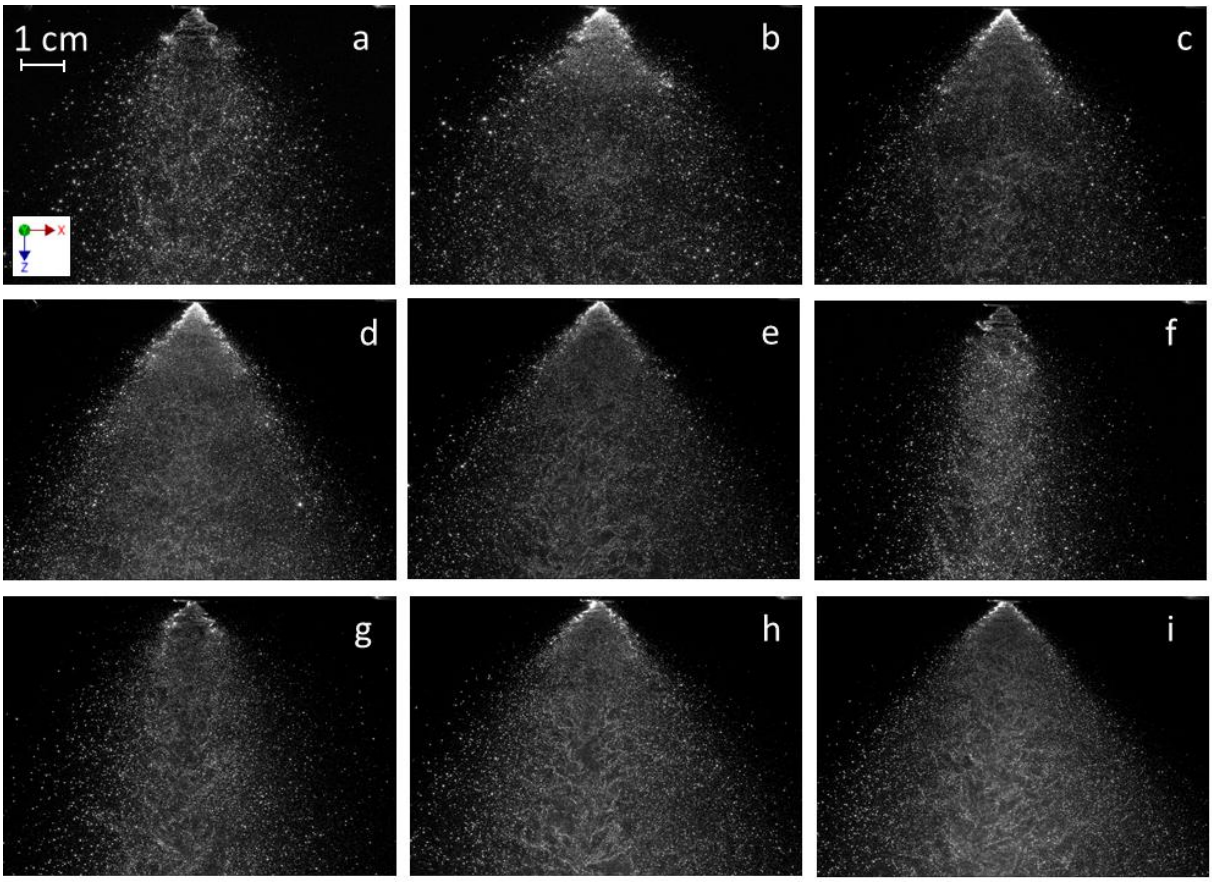

Figure 5 Spray visualizations: a) N1 200/50 kPa; b) N1 340 kPa; c) N1 690 kPa; d) N1 1000 kPa; e) N1 1000/400 kPa; f) N2 200 kPa; g) N2 340 kPa; h) N2 690 kPa; i) N2 1000 kPa.

its thickness. The liquid sheet disintegrates into ligaments and drops in a very short distance from the nozzle orifice in the form of a well-defined hollow-cone spray (Fig. 5h, 5i). This behaviour is consistent with other simplex nozzles described in the literature [3, 6–9]. Inspection of Figs. 5g to 5i indicates that the spray core is formed by smaller droplets, and in the radial distance droplet size increases. Droplet clusters can be seen in the spray core as the result of the interaction of droplets with the ambient air. Cone angle increases at first rapidly with increasing inlet pressure. At inlet pressure values above 600 kPa, cone angle increases slowly towards its final value defined by the internal geometry (reached at around 1 MPa).

Table 2 Spray cone angle 2θ for different operating regimes.

Operating regime	Nozzle 1	Nozzle 2
1	80° (a)	60° (f)
2	74° (b)	78° (g)
3	76° (c)	86° (h)
4	76° (d)	88° (i)
5	86° (e)	-

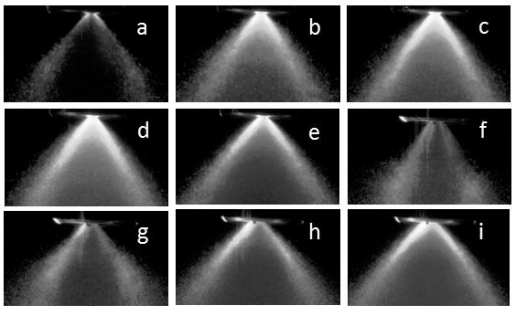

Figure 6 Averaged PIV captures for spray cone angle measurement.

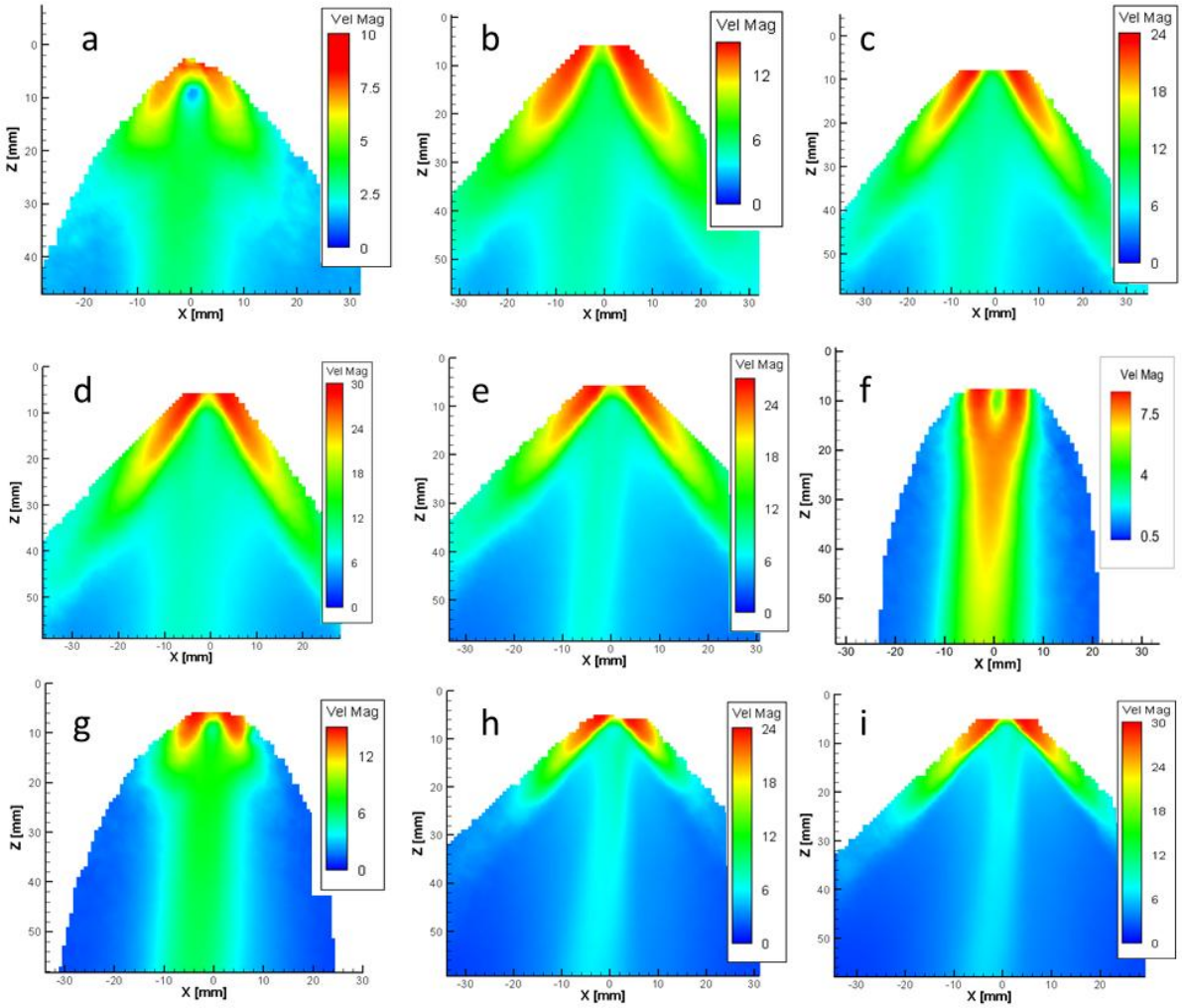

Figure 7 Velocity magnitudes: a) N1 200/50 kPa; b) N1 340 kPa; c) N1 690 kPa; d) N1 1000 kPa; e) N1 1000/400 kPa; f) N2 200 kPa; g) N2 340 kPa; h) N2 690 kPa; i) N2 1000 kPa.

Processed PIV captures provide visualization of the droplet velocity magnitude in the whole field of view (Fig. 7). Labelling of the various regimes corresponds to the labelling in Figure 5 and 6. Velocity distribution in the spray generated by Nozzle 1 indicates a hollow cone formation from the low inlet pressure up to the maximum pressure setting. In the spill-controlled regime, Nozzle 1 generates finer droplets, which due to their lower kinetic energy decelerate in a short distance downstream from the discharge orifice (Fig. 7a). Sprays generated in the regimes 2–4 have similar spatial velocity distribution, differing in the velocity magnitude in the proximity of the nozzle orifice (Fig. 7b–7d). As we can see in Figure 7e, spray generated in the spill-controlled regime at 1000 kPa inlet pressure exhibits lower velocity magnitude of droplets than the regime without spill return at the same inlet pressure, what is related to the lower thickness of the liquid sheet and thus the smaller droplets.

Velocity magnitude distribution in sprays generated by Nozzle 2 shows a significant dependence on the inlet pressure for regimes 1 and 2 (Fig. 7f, 7g). For the lowest pressure, fluid mass is concentrated around the spray axis; high velocity region is located under the break-up spot of the liquid sheet bubble. With increasing gauge pressure, spray mass shifts towards the spray periphery. Droplet dynamics leads to deformation of the velocity profile with increasing axial distance. Influence of the ambient air leads to significant deceleration of drops with increasing distance from the nozzle orifice. For inlet pressures above 340 kPa, Nozzle 2 generates a hollow-cone spray. Although the spray core is formed by a large number of small drops, due to their small volume represents the mass flux in the central area only a fraction of the total mass flux in the axial direction. With increasing gauge pressure, cone angle increases first significantly (Fig. 7f, 7g) and then only moderately (Fig. 7h, i), what is evident from the spray photographs, as well.

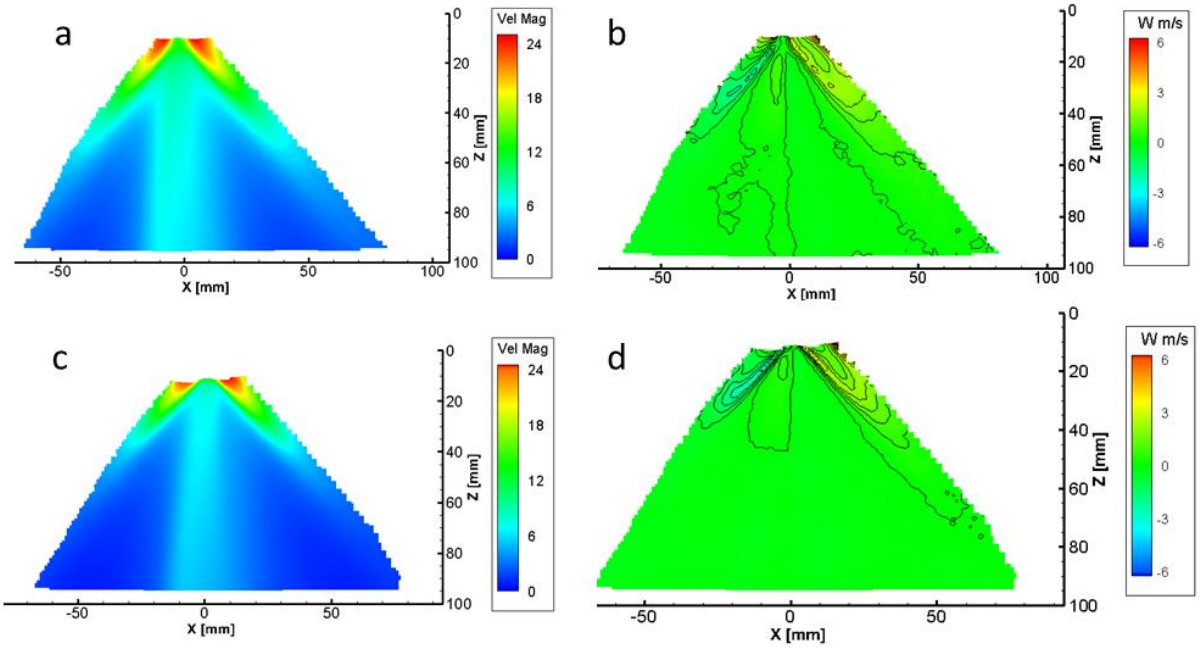

Figure 8 Velocity vector fields obtained from the stereoscopic PIV: a) N1 1000/400 kPa, velocity magnitude; b) N1 1000/400 kPa, out-of-plane velocity component estimate; c) N2 1000 kPa, velocity magnitude; b) N2 1000 kPa, out-of-plane velocity component estimate.

Stereoscopic PIV measurements were carried out in order to investigate the extent to which the out-of- plane velocity component influences the velocity magnitude and turbulence when compared to the results obtained with single-camera results. For the purpose of this paper, comparison of the velocity magnitudes and estimates of the tangential velocity components obtained from stereoscopic PIV are shown in Figure 8. In this figure, we can find a comparison of the velocity magnitudes (8a, 8c) and the out-of-plane velocity components (tangential velocity components) for Nozzle 1 in operating regime 5 and Nozzle 2 in operating regime 4. It can be seen that the velocity distribution in Fig. 8a and 8c corresponds to the single-camera results presented in Fig. 7. Tangential velocity component of droplets is expected to attain the highest values downstream after the breakup of the liquid sheet when the droplets are still driven by the angular momentum of the swirling liquid. This behaviour was confirmed by our measurements (Fig. 8b, 8d). Spray droplets at the spray periphery in a short distance from the discharge orifice exhibit a tangential displacement in respect to the spray axis. However, influence of this velocity component on the velocity magnitude seems to be insignificant since the estimated tangential velocity was of

one order of magnitude lower than the axial velocity component in this region of the spray cone. With increasing downstream distance, tangential velocity was close to zero.

Figures 9–12 give the results of PDA measurements of Sauter mean diameter (SMD) and the axial droplet velocity taken at z = 50 mm downstream from the nozzle orifice. In our particular interest were the results of the spill-controlled regimes of Nozzle 1 compared to the regimes without spill return. Comparing the axial droplet velocity at 200/50 kPa and 150 kPa, a slight decrease can be observed for the former regime. This is caused by the lower kinetic energy of droplets generated in this regime. With increasing inlet pressure up to 700 kPa, SMD values decrease significantly in the centre. Further increase in pressure does not affect SMD significantly. However, in the spill-controlled regime 1000/400 kPa we can see that the SMD of droplets in the centre drops below the SMD values at 1000 kPa. Droplet velocity at 1000/400 kPa drops markedly below the values at 1000 kPa. Increase of spray cone angle causes that the velocity maxima in this regime are shifted to larger radial distances from the centre (see Fig. 10).

SMD of droplets in case of Nozzle 2 changes significantly with increasing gauge pressure and radial distance (Fig. 11). For low pressure, particles with the greatest diameter are concentrated close to the spray axis (area of the greatest mass flux). For low inlet pressures, droplets reach the highest velocity magnitude in the centre. With increasing pressure differential, local velocity maxima at the spray periphery are dominant.

These results are consistent with the results of PIV measurements presented above. It can be seen that both nozzles exhibit a different behaviour with changes in pressure differential.

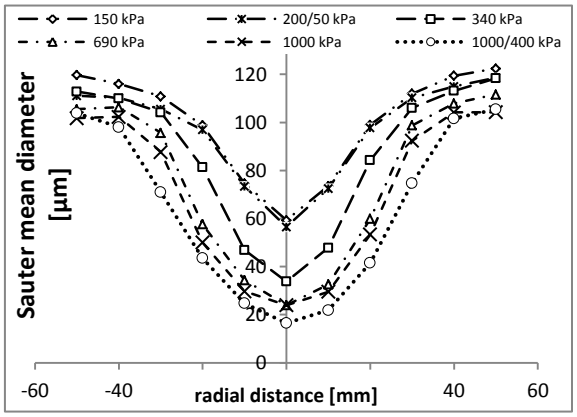

Figure 9 Nozzle 1**;** Sauter mean diameter.

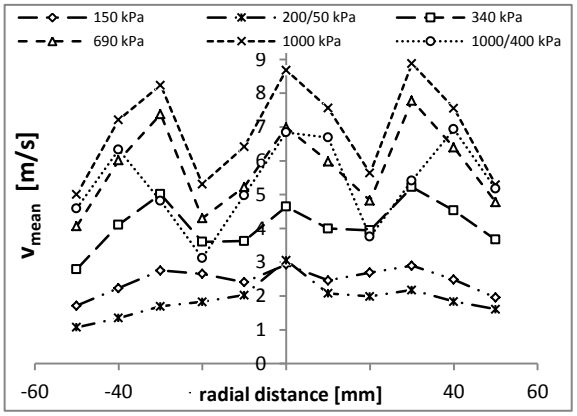

Figure 10 Nozzle 1; axial velocity.

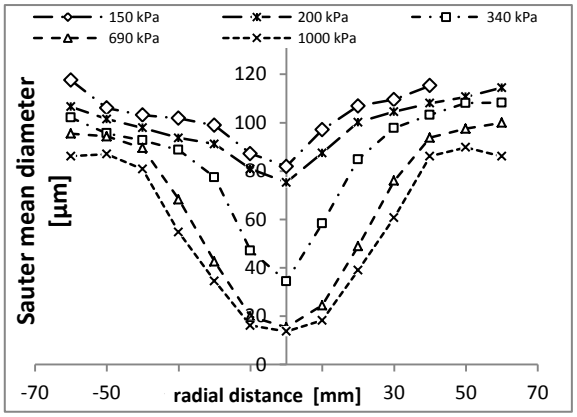

Figure 11 Nozzle 2; Sauter mean diameter.

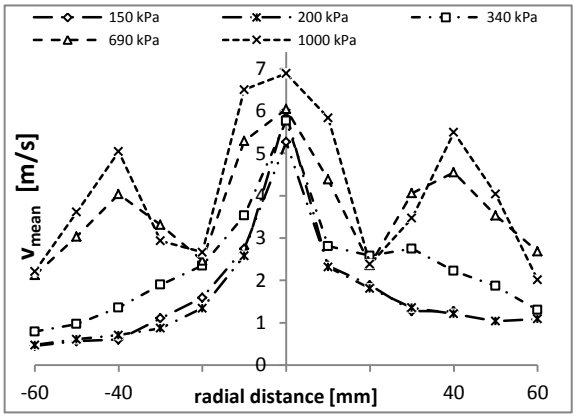

Figure 12 Nozzle 2; axial velocity.

Summary and Conclusions

In the present work, mean size and velocity of droplets generated with two geometrically different pressure-swirl atomizers for a combustion chamber of a small-sized jet engine are obtained using two optical diagnostic techniques – Particle Image Velocimetry and Phase-Doppler Anemometry. The former nozzle (Nozzle 1) is a spill-return type and the latter one is a newly designed simplex nozzle without spill return (Nozzle 2). It was observed that these nozzles generate sprays with different quality and morphology when compared for the same operating conditions. Nozzle 1 generates a hollow cone spray with only moderate increase in spray cone angle

with increasing inlet pressure. Following effects of spill fuel flow on atomization quality were observed: drop-size distribution in spill-controlled operating regimes is shifted towards lower values of the Sauter mean diameter; spray cone angle increases with an increase of the fraction of the fuel spilled from the swirl chamber; droplet velocity is lower due to the decrease of the liquid sheet thickness. Spray characteristics of Nozzle 2 were found to be highly dependent on fuel injection pressure. For lower values below 300 kPa, the nozzle generates a full cone spray with the liquid mass concentrated in the centre and with increasing pressure changes into a hollow cone spray. Investigated differences in spray characteristics will most likely cause different behaviour of the nozzles in the combustion chamber. Different spray geometry, drop-size and velocity distribution will cause different interaction of the fuel with ambient air, evaporation rate and subsequent heat release during the combustion process. The new nozzle will also have different requirements on engine power regulation. It is most likely that the original combustion chamber optimized for the spill-return nozzle will require design optimization for the new nozzle.

Further research will focus on optimization of the PIV measurements and application of advanced processing algorithms and decomposition methods.

Acknowledgements

Authors greatly acknowledge financial support from project No. 101/11/1264 funded by the Czech Science Foundation and from Operational Programme "Research and Development for Innovations" – "NETME Centre – New Technologies for Mechanical Engineering" Reg. No. CZ.1.05/2.1.00/01.0002.

References

[1] Quentin, F., *ACARE: the European Technology Platform for Aeronautics*, December 2007. Available online: ftp://ftp.cordis.europa.eu/pub/etp/docs/acare_en.pdf
[2] Lefebvre, A. H., Ballal, D. R., *Gas Turbine Combustion*, 3rd edition, CRC Press, 2010.
[3] Lefebvre, A. H., *Atomization and Sprays*, Hemisphere Publishing, 1989.
[4] Taylor, G. I., *Seventh International Congress of Applied Mechanics* 2 (1948).
[5] Squire, H. B., *British Journal of Applied Physics* 4: 1697-1969 (1953).
[6] Rizk, N. K., Lefebvre, A. H., *Journal of Propulsion and Power* 1:193-199 (1985).
[7] Rizk, N. K., Lefebvre, A. H., *ICLASS-85 Proceedings* (1985).
[8] Wang, X. F., Lefebvre, A. H., *Atomisation and Spray Technology* 3 (1987).
[9] Wang, X. F., Lefebvre, A. H., *Journal of Propulsion and Power* 3-1: 11-18 (1987).
[10] Chu, C., Chou, S., Lin, H., and Liann Y., *Heat and Mass Transfer* 45: 11-22 (2008).
[11] Muliadi, A.R, Sojka, P. E., Sivathanu, Y. R. and Lim, J., *Journal of Fluids Engineering, Transactions of the ASME* 132-6: 061402-061412 (2010).
[12] Belhadef, A., Vallet, A., Amielh, M. and Anselmet, F. *Int. Journal of Multiphase Flow* 39: 13-20 (2011).
[13] Kohse-Hoeinghaus, K., Jeffries, J. B. (Ed.), *Applied Combustion Diagnostics*, Taylor&Francis, 2002.
[14] Li, T., Nishida, K. and Hiroyasu, H., *Fuel* 90-7: 2367-2376 (2011).
[15] Yao, Sh., Zhang, J., Fang, T., *Experimental Thermal and Fluid Science* 39: 158-166 (2012).
[16] Carey, F. H. *Journal of the Royal Aeronautical Society* 58 (1954)
[17] Rizk, N. K., Lefebvre, A. H., *Journal of Propulsion and Power* 1-1:16-22 (1985).
[18] Rizk, N. K., Lefebvre, A. H., *Journal of Propulsion and Power* 1-3:200-204 (1985).
[19] Nasr, G. G., Yule, A. J., Stewart, J. A., Whitehead, A. and Hughes, T., *Proceedings of the 21th ILASS-Europe Meeting* (2007).
[20] Adrian, R. J., Westerweel, J., *Particle Image Velocimetry*, Cambridge University Press, 2011.